Lattice deformation of a silver nanocube under high pressure

Xiaojing Huang,[1,2] Wenge Yang,[1] Ross Harder,[3] Yugang Sun,[4] Ming Lu,[5] Yong S. Chu,[2] Ian K. Robinson,[6,7] and Ho-kwang Mao[1,8]

[1]*HPSynC, Carnegie Institution of Washington, Argonne, IL 60439, USA*
[2]*National Synchrotron Light Source II, Brookhaven National Laboratory,Upton, NY 11973, USA*
[3]*Advanced Photon Source, Argonne National Laboratory, Argonne, IL 60439, USA*
[4]*Center for Nanoscale Materials, Argonne National Laboratory, Argonne, IL 60439, USA*
[5]*Center for Functional Nanomaterials, Brookhaven National Laboratory,Upton, NY 11973, USA*
[6]*London Centre for Nanotechnology, University College London, London, WC1H 0AH, UK*
[7]*Research Complex at Harwell, Didcot, Oxfordshire OX11 0DE, UK*
[8]*Geophysical Laboratory, Carnegie Institution of Washington, Washington, DC 20015, USA*

(Dated: September 10, 2013)

The developments of local lattice distortion and bulk morphology deformation of a single-crystal silver nanocube under high-pressure environment were investigated using Bragg coherent diffraction imaging (Bragg CDI) method. The measurements were conducted with silver nanocubes sealed in a diamond anvil cell using water as the pressure transmitting medium. The three-dimensional (3D) data were collected at 2.1 GPa, when water transformed to a high-density solid ice-VII phase. We demonstrate that the water solidification process mitigated both translation and rotation degree of freedoms of the nanocrystal sample, which is necessary for high resolution 3D data acquisition. A significant crystal shape deformation caused by a shear stress was recovered from reconstructed image.

PACS numbers: 61.05.cp, 87.59.-e, 61.46.-w, 07.35.+k

The capability to apply adjustable high-pressures onto specimens under investigation introduces an additional dimension onto materials' phase diagrams and enriches their characteristics. Tremendous novel properties [1–3] and new forms of materials [4] have been revealed exclusively under high-pressure. Measuring and understanding the internal strain response to the external pressure produces critical information to unveil the origin of unconventional behavior of crystalline materials in high-pressure environments.

Nanoscale crystals show abnormal properties compared with their bulk counterparts [5, 6]. It is crucial to develop a nanoscale probe to reveal strain field inside individual nanocrystals. Bragg CDI provides this unique capability to image the shape and the lattice distortion field inside nanocrystals with high spatial resolution and high sensitivity through local atomic displacements by collecting diffraction patterns in the vicinity of Bragg condition [7]. A typical Bragg CDI measurement requires a crystal with proper dimensions to satisfy stringent sampling criterion [8, 9]. The crystalline sample is also compelled to be stabilized during 3D data acquisition over a period of time from a few minutes to a few hours. For nanocrystals, significant translational and rotational motions were observed when a free-standing crystal is illuminated by an intense X-ray beam, due to a number of possible reasons including electric repulsive force after ionizing, differential light pressure from the illumination intensity gradient, or the mechanical momentum transfer vector associated with Bragg reflection. The method usually requires specimens strongly attached to substrates [7, 10–13]. Recently, the bond-to-substrate strategy was successfully applied to Bragg CDI measurement in high-pressure environment [14], where the nanocrystals were prepared by being annealed on and thus well attached to a silicon substrate. Crystals, together with their substrate, were loaded into a diamond anvil cell (DAC), and the strain and morphology evolutions of a gold nanocrystal were tracked under various high-pressure conditions.

In the present work, we explore a different approach to stabilize nanocrystal specimens for high-pressure studies by sealing them in a solid medium. We chose water as the pressure transmitting medium, because liquid water transforms to solid state at a relatively low pressure ($\sim$ 0.9 GPa) at room temperature [15, 16]. The experimental result confirms that the solidification process significantly slowed down the sample motion and enabled 3D Bragg CDI data acquisition. A shear stress and the associated crystal deformation were observed from the reconstructed images.

The specimens imaged in this experiment are single-crystal silver nanocubes. They were synthesized from ethylene glycol solution of silver nitrate in the presence of poly-vinyl-pyrrolidone (PVP) [17]. Tuning the molar ratio of PVP with respect to silver nitrate controls the shape and size of the final precipitate products. With a molar ratio of 1.5 between PVP and $AgNO_3$, single crystalline silver nanocubes can be obtained. Cubic silver crystals with 120 nm mean edge length were used in this experiment. Fig. 1 shows the scanning electron microscope (SEM) picture of these silver nanocubes. They contain six {100} planes on their surface, the plane edges are truncated to {110} facets, and the corners form small {111} facets, as shown in the inset of Fig. 1.

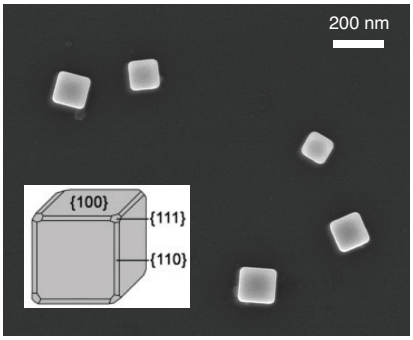

FIG. 1: SEM image of silver nanocubes imaged in this experiment.

The silver nanocubes suspended in de-ionized water were loaded into a panoramic DAC equipped with a pair of diamond anvils with 500 μm culet size. The beryllium gasket was pre-indented to about 70 μm, and a 200 μm hole was drilled for serving as a sample chamber. Silver nanocubes and several ruby balls were loaded inside the sample chamber. The pressure measurement was quantified *in-situ* from the fluorescence line shift of ruby crystals [18]. Upon the initial sealing of the DAC, the pressure was found to have stabilized at 1.5 GPa.

The Bragg CDI measurement was performed at Beamline 34-ID-C of Advanced Photon Source at Argonne National Laboratory. The DAC, loaded with silver nanocubes, was mounted at the rotation center of the diffractometer. A 9 keV coherent X-ray beam, selected by silicon (111) double-crystal monochromator, was focused by a pair of K-B mirrors down to about 1.5 μm (full-width-at-half-maximum or FWHM) [19]. The incident X-rays penetrated the beryllium gasket and illuminated the samples. A ruby fluorescence spectroscopy system was installed by the diffractometer, which enables *in-situ* pressure monitoring without removing DAC for pressure adjustment. A direct-detection charge-coupled device (CCD) with 20 μm$\times$20 μm pitch was placed 0.7 m away and oriented for the silver (111) Bragg angle.

Although the water sealed inside DAC was expected to be solid ice-VI phase at 1.5 GPa [16, 20], significant sample drifting and rotation were observed through tracking Bragg peak positions on the CCD detector. A previous study showed that the ice-VI phase has finite viscosity, and this value decreases to its minimum at the triple point of ice-VI and ice-VII [21]. The relatively low viscosity in our measurement condition allowed that nanocubes had freedom to move and/or rotate. Some silver (111) Bragg peaks brightened up or dimmed, which is a signature of sample drifting in and out of the X-ray beam. Some Bragg peaks traveled along the silver (111) powder ring or rocked across the Bragg peak center, which indicates that the crystal spun along different axes. The Bragg peak positions with sequential X-ray exposures were followed under various pressure conditions.

The drifted distances of Bragg peaks are shown in Fig. 2 (a). At 1.5 GPa and 1.8 GPa, the Bragg disappeared on CCD within 2 minutes of X-ray illumination. At 2.1 GPa, ice-VI started to transform to high-density ice-VII phase [22], and the crystal drifting was significantly slowed down. After increasing pressure to 2.9 GPa, the sample became stabilized. However, this high pressure deformed the silver nanocrystals aggressively enough to deform their initial cubic shape, so that no interference fringes could be found.

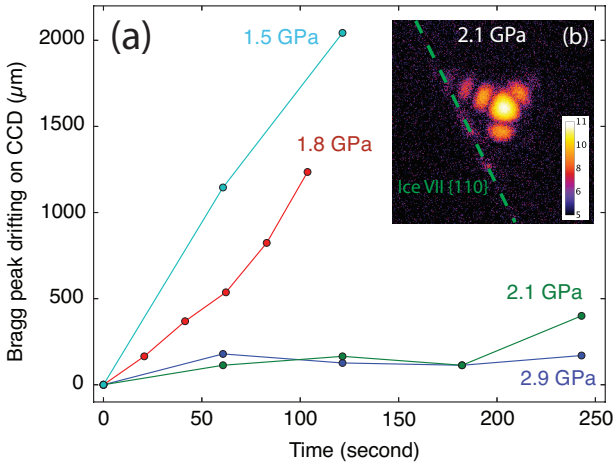

FIG. 2: (a) Silver (111) Bragg peak drifted on CCD detector with sequential X-ray illumination. The drifting rate slowed down with increasing pressure. (b) A typical diffraction pattern from a silver nanocube at 2.1 GPa.

Among the 4 examined pressure conditions, 2.1 GPa appears to provide an optimized combination of sample stability and morphology (as shown in Fig. 2 (b)) for 3D Bragg CDI data collection. However, not all crystals were stabilized under 2.1 GPa. We found that crystals, whose orientation well satisfied the Bragg condition, moved rapidly, while the ones which were slightly off the Bragg peak, kept their position reasonably well up to about 10 minutes. This observation implies that the momentum transfer dominates the driving effect on these silver nanocubes. The relatively slow migration of Bragg peak at 2.1 GPa also suggested that the crystal was under a continuous deformation process, as was verified by repeated measurements.

We measured the Bragg CDI signal from a (111) peak from a silver nanocube under 2.1 GPa pressure environment. The 3D diffraction data spans 0.4 degree angular range with 0.02 degree angular steps. The CCD pixels were 2 $\times$ 2 binned to increase signal statistics. In order to collect high resolution data within moderate time interval, each frame accumulated three 10-second exposures. The entire data acquisition took about 10 minutes within the stable time range. The final cropped data size was 96 $\times$ 96 $\times$ 32, which gave a real space voxel size of 11 $\times$ 11 $\times$ 20 nm^3. The d-spacing of silver {111} planes

is 2.359 Å, which is very close to the {110} d-spacing of high-density ice-VII phase, 2.365 Å [23]. The powder ring of ice-VII polycrystal was located in the vicinity of the silver (111) peak, as shown in Fig. 2 (b). This ice powder ring signal was masked before feeding the data into the reconstruction algorithm. The phase retrieval process was started with 40 error-reduction (ER) iterations [24, 25], followed by 420 iterations of hybrid-input-output (HIO) algorithm [26], and finished with another 40 ER iterations. $[-\pi/2, \pi/2]$ phase-constraint [27] was enforced in the HIO iterations to accelerate convergence. The shrink-wrap method [28] was also applied to refine a tight support. Partial coherence deconvolution [29] was utilized to separate artifacts from incoherent scattering sourced from upstream optics and adjacent sample environments [14]. Fig. 3 (a) and (b) show the reconstructed magnitude of the silver nanocube. The obtained crystal size was about 120 nm, which is consistent with the dimension range from the SEM measurement as shown in Fig. 1. Fig. 3 (c) plots the central line along the x direction, whose derivative on its raising side was fitted by a Gaussian function and gave a FWHM width of 41 nm (Fig. 3 (d)).

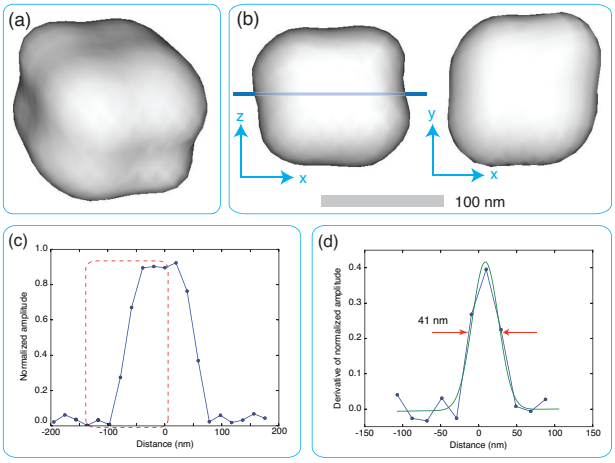

FIG. 3: (a) 3D iso-surface rendering of the reconstructed magnitude of a silver nanocube. (b) Side view and bottom view of the reconstructed magnitude measured at 2.1 GPa. (c) A line plot along x-axis across the cubic center indicated by the blue horizontal line in (b). (d) Gaussian fit to the derivative of the raising side of the line plot gives 41 nm FWHM width.

To track the continuing strain and morphology developments of the same nanoparticle, the identical measurement was repeated twice, in 15 minutes and 1 hour, respectively. Fig. 4 shows the reconstructed images, where the crystal shape deformation is clearly shown, especially for the last measurement. The overall phase shift range is within $[-\pi/6, +\pi/6]$. Relatively strong phase features are found at the cube corners and edges in the image from the first measurement. The phase pattern was evolved within 15 minutes, with roughly the same distribution but reduced phase values. It suggests that the strain level was decreased during crystal shape deformation, which is consistent with the observation on gold nanocrystals [14]. Considering that it took about 20 minutes to find this crystal after tuning up pressure, one can expect that this silver nanocrystal had even higher phase values right after pressure adjustment. The crystal was dramatically distorted after 1 hour, to an elongated shape. In the mean time, the crystal strain level was further released. The crystal volume was reduced by 50% compared with the previous 2 measurements. This implies that portions of the initial crystal cube were sufficiently deformed to form smaller grains oriented along different directions.

The top surfaces of the reconstructed images from the first 2 measurements are dominated with positive phases, while the bottom surfaces are mainly negative phases. Since the recovered phase in Bragg CDI method is determined by lattice displacement projected on the $\vec{Q}$ vector direction [30], this phase distribution suggests that the silver nanocube was experiencing an expansion along the vertical direction. The silver nanocubes embedded in non-hydrostatic pressure medium encountered shear stress around them, which originated the observed anisotropic deformation.

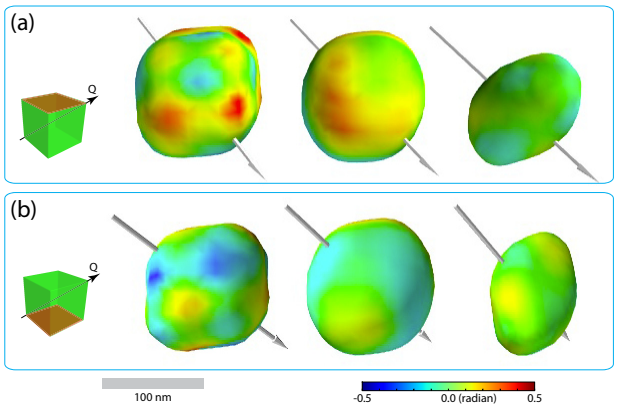

FIG. 4: The top view (a) and bottom view (b) of reconstructed images of the same silver nanocube from repeated measurements at time zero (the second column), 15 minutes later (the third column), and 1 hour later (the fourth column), with recovered phases coated on 20% isofurfaces. The arrow points the $\vec{Q}$ vector direction.

The silver crystal distortion was also directly manifested onto the internal phase structure of the reconstructed image. Fig. 5 (a) shows a phase slice of the reconstruction from the second measurement on a $(0\bar{1}1)$ plane, as indicated by the insert. The phases on this plane were well separated into 2 areas, almost equally divided by the [111] $\vec{Q}$ vector: the top-left half with positive phases, the bottom-right with negative phases. To ensure this phase separation represents the intrinsic crystal lattice distortion, we eliminated the phase ramp from mis-centering of diffraction pattern. The complex-valued

reconstructed image $Ae^{i\phi}$ and its amplitude part A were Fourier transformed to reciprocal space. FT$[Ae^{i\phi}]$ was then aligned with FT$[A]$ with 0.01 pixel accuracy using the discrete-Fourier-transform-based sub-pixel registration method [31]. Inverse Fourier transforming the aligned FT$[Ae^{i\phi}]$ back to real space gave final images with the overall phase ramp removed.

The phase splitting was found to be separated by a $(1\bar{1}\bar{1})$ plane crossing the nanocube center. Phases in the half volume above the central $(1\bar{1}\bar{1})$ plane are positive, while those in the other half are negative. Fig. 5 (b) and (c) display two $(1\bar{1}\bar{1})$ phase cut planes above and below the $\vec{Q}$ vector, respectively. This phase distribution indicates that the top half volume has positive lattice distortion component along $\vec{Q}$ direction, while the bottom half is opposite, as shown in Fig. 5 (d). As a result, a plane slip deformation was formed at the phase division interface. For face centered cubic crystals, slip displacement usually occurs along the close packed {111} plane. In the silver nanocube measured in our experiment under non-hydrostatic high pressure environment, the local shear stress inhomogeneity introduced slip indeed took place on a {111} plane.

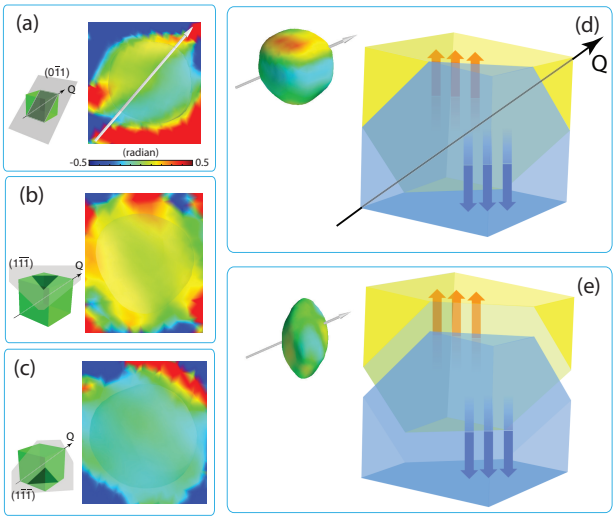

FIG. 5: Phase shift map of the silver nanocube measured at 2.1 GPa. (a) The central phase slice on $(0\bar{1}1)$ plane. (b) (c) Phase distributions on two $(1\bar{1}\bar{1})$ planes with about 30 nm above and below the cube center, respectively. (d) The internal phase distribution indicates that the nanocube was divided by a $(1\bar{1}\bar{1})$ plane into 2 oppositely deforming parts. (e) Continuous deformation along the $(1\bar{1}\bar{1})$ plane towards opposite directions results in the elongated crystal shape as observed in the third measurement.

The shear stress generating the observed distortion pattern can be estimated from the reconstructed phase values. For the second measurement, the averaged phases ϕ of the separated volumes are about $+0.15$ and -0.15 radians, respectively. During the slip deformation process, one can expect that the main lattice displacement takes place in the slipping plane. In our case, the mostly possible slip directions are along six <110>-type directions: [110], [101], $[01\bar{1}]$ and their reversions, which are perpendicular to the slip plane normal $[1\bar{1}\bar{1}]$ direction. Among these directions, displacements in $[01\bar{1}]$ and $[0\bar{1}1]$ are not sensitive to the measurement because they are perpendicular to the [111] $\vec{Q}$ vector, displacements in [110] and [101] have positive components on the $\vec{Q}$ direction so that they are the possible displacements for the top half crystal volume, displacements in $[\bar{1}\bar{1}0]$ and $[\bar{1}0\bar{1}]$ are for the bottom half volume that give negative components on $\vec{Q}$. Considering that the obtained phases determines the displacement component projected on to the [111] $\vec{Q}$ vector direction and the angle θ between $\vec{Q}$ and possible <110> directions is about 35 degree, the lattice displacement can be calculated as $\Delta x \cos\theta = d \cdot \phi/2\pi$. The corresponding shear stress σ can be estimated as $\sigma = G\Delta x/d$ [32], where d is the d-spacing of planes under investigation and G is the shear modulus of the silver nanoparticle. Using the typical shear modulus of silver 30 GPa [33] and 0.15 radian phase shift, the estimated shear stress is about 0.88 GPa. The theoretical elastic limit of shear strength is about $G/30$ [34], which is about 1 GPa for silver. As the estimated shear stress value was slightly below the elastic limit stress, the nanocube can hold the shape during the first and second measurements.

The pressure inside the DAC was gradually climbing during the repeated measurements. The pressure reading from the ruby fluorescence spectroscopy system was increased from 2.1 GPa to 2.4 GPa before we tuning pressure to next level. At some point between the second and third measurements, the local lattice strain exceeded the elastic limit. The {111} <110> slip system was activated, and a plastic deformation occurred. Through the dislocation slip crossing the crystal, the local elastic strain was released to lower level, and the crystal shape was elongated to an elliptical shape, as seen from the third measurement (shown in Fig. 5 (e)).

Further attempts were performed to measure the same crystal, but the Bragg peak was found to be in an unstable state again. One can expect that the deformation kept going on, and the nanocube turned to a narrow-long oval shape.

In conclusion, the solidification process of pressure transmitting medium was demonstrated to retain the position and orientation of nanoscale crystals sufficiently for 3D Bragg CDI measurement. The morphology and lattice distortion of a silver nanocube were obtained from the reconstructed amplitude and phase, respectively. Sequential measurements were conducted at 2.1 GPa with nanocubes embedded in solid ice VII phase inside a DAC. The slip deformation deduced from the recovered phase distribution was consistent with its altered reconstructed shape.This method can be directly applied onto other nanocrystal specimen and pressure transmitting medi-

ums with similar properties. It provides a new approach for morphology and strain studies under a high pressure environment with Bragg CDI or other techniques requiring steady samples.

This work was supported by EFree, an Energy Frontier Research Center funded by DOE-BES under Grant number DE-SC0001057. I.K.R. is supported by the ERC "nanosculpture" advanced grant 227711. Y.S.C. is supported by Brookhaven Science Associates, LLC under contract no. DE-AC02-98CH10886. The measurements were carried out at APS beamline 34-ID-C, built with US National Science Foundation grant DMR-9724294 and operated by the US Department of Energy, Office of Basic Energy Sciences, under contract no. DE-AC0206CH11357.

[1] C. Guillaume, E. Gregoryanz, O. Degtyareva, M. McMahon, M. Hanfland, S. Evans, M. Guthrie, S. Sinogeikin, and H. Mao, Nature Physics **7**, 211 (2011).
[2] L. Sun, X. Chen, J. Guo, P. Gao, Q. Huang, H. Wang, M. Fang, X. Chen, G. Chen, Q. Wu, et al., Nature **483**, 67 (2012).
[3] M. Somayazulu, P. Dera, A. Goncharov, S. Gramsch, P. Liermann, W. Yang, Z. Liu, H. Mao, and R. Hemley, Nature Chemistry **2**, 50 (2010).
[4] M. Eremets and I. Troyan, Nature Materials **10**, 927 (2011).
[5] S. Tolbert and A. Alivisatos, Science **265**, 373 (1994).
[6] Q. Gu, G. Krauss, W. Steurer, F. Gramm, and A. Cervellino, Physical Review Letters **100**, 045502 (2008).
[7] M. Pfeifer, G. Williams, I. Vartanyants, R. Harder, and I. Robinson, Nature **442**, 63 (2006).
[8] D. Sayre, Acta Crystallographica **5**, 843 (1952).
[9] J. Miao, D. Sayre, and H. Chapman, The Journal of the Optical Society of America A **15**, 1662 (1998).
[10] G. Williams, M. Pfeifer, I. Vartanyants, and I. Robinson, Physical Review Letters **90**, 175501 (2003).
[11] M. Newton, S. Leake, R. Harder, and I. Robinson, Nature Materials **9**, 120 (2010).
[12] P. Godard, G. Carbone, M. Allain, F. Mastropietro, G. Chen, L. Capello, A. Diaz, T. Metzger, J. Stangl, and V. Chamard, Nature Communications **2**, 568 (2011).
[13] X. Huang, R. Harder, S. Leake, J. Clark, and I. Robinson, Journal of Applied Crystallogrphy **45**, 778 (2012).
[14] W. Yang, X. Huang, R. Harder, J. Clark, I. Robinson, and H. Mao, Nature Communications **4**, 1680 (2013).
[15] A. Lyapin, O. Stal'gorova, E. Gromnitskaya, and V. Brazhkin, Journal of Experimental and Theoretical Physics **94**, 283 (2002).
[16] M. Choukroun and O. Grasset, The Journal of Chemical Physics **127**, 124506 (2007).
[17] Y. Sun and Y. Xia, Science **298**, 2176 (2002).
[18] H. Mao, J. Xu, and P. Bell, Journal of Geophysical Research **91**, 4672 (1986).
[19] X. Huang, M. Wojcik, N. Burdet, I. Peterson, G. Morrison, D. Vine, D. Legnini, R. Harder, Y. Chu, and I. K. Robinson, Optics Express **20**, 24038 (2012).
[20] B. Kamb, Science **150**, 205 (1965).
[21] V. Mineev and A. Funtikov, High Temperature **43**, 141 (2005).
[22] G. Johari, A. Lavergne, and E. Whalley, Journal of Chemical Physics **61**, 4292 (1974).
[23] W. Kuhs, J. Finney, C. Vettier, and D. Bliss, Journal of Chemical Physics **81**, 3612 (1984).
[24] R. Gerchberg and W. Saxton, Optik **35**, 237 (1972).
[25] J. Fienup, Optics Letters **3**, 27 (1978).
[26] J. Fienup, Applied Optics **21**, 2758 (1982).
[27] R. Harder, M. Liang, Y. Sun, Y. Xia, and I. Robinson, New Journal of Physics **12**, 035019 (2010).
[28] S. Marchesini, H. He, H. Chapman, S. Hau-Riege, A. Noy, M. Howells, U. Weierstall, and J. Spence, Physical Review B **68**, 140101 (2003).
[29] J. Clark, X. Huang, R. Harder, and I. Robinson, Nature Communications **3**, 993 (2012).
[30] I. Robinson and R. Harder, Nature Materials **8**, 291 (2009).
[31] M. Guizar-Sicairos, S. Thurman, and J. Fienup, Optics Letters **33**, 156 (2008).
[32] C. Kittel, *Introduction to Solid State Physics* (Wiley, 2004), 8th ed.
[33] G. Kaye and T. Laby, *Tables of Physical and Chemical Constants* (Longmans, London, 1993), 15th ed.
[34] D. Mackenzie and J. Boyle, International Journal of Pressure Vessels and Piping **53**, 77 (1993).